Monte Carlo computations of the quantum kinetic energy of rare-gas solids

Alessandro Cuccoli, Alessandro Macchi, and Valerio Tognetti
Dipartimento di Fisica dell'Università di Firenze, Largo Enrico Fermi 2, I-50125 Firenze, Italy

Ruggero Vaia
Istituto di Elettronica Quantistica del Consiglio Nazionale delle Ricerche, Via Panciatichi 56/30, I-50127 Firenze, Italy
(Received 9 November 1992)

We report results from Monte Carlo computations for the average kinetic energy of rare-gas solids (neon, argon, krypton, and xenon), modeled by a Lennard-Jones all-neighbor interaction. The main motivation lies in the recent availability of direct experimental measurements of the average kinetic energy of solid neon, by means of deep-inelastic neutron scattering (DINS). In our computations we take strong advantage in using the effective potential technique, which has been proven to be very useful for systems where quantum effects are not too strong: the *path-integral* Monte Carlo (PIMC) can be replaced by the classical-like *effective-potential* Monte Carlo (EPMC), in such a way that the needed computer time is strongly reduced. We resorted to PIMC in the case of neon, due to its rather high quantum effects. Our results for the low-temperature kinetic energy of neon are smaller than the measured ones. This discrepancy could be attributed to the simple model of the interaction we have used, as the agreement with previous theoretical calculations suggests. Moreover, we show that the quantum contributions to the kinetic energy, at the same temperatures used in the above-mentioned experiments, are unexpectedly relevant also for argon, krypton, and xenon crystals, so that they should be experimentally detectable as well.

I. INTRODUCTION

Deep-inelastic neutron scattering (DINS) (Refs. 1–4) is an experimental technique, based on the inelastic diffusion of very energetic neutrons (~ 1 eV) at large momentum transfer, that has become very effective in the last decade, thanks to the availability of intense spallation neutron sources. DINS experiments on liquids and solids allow us to get direct information on single-particle momentum distributions. This is apparent in the so-called *impulse approximation*, where the momentum transfer $k \to \infty$: in this limit each scattering atom recoils as if it were free, and if $\boldsymbol{p}$ is its initial momentum, the conservation of energy and momentum requires that $\hbar\omega = (\boldsymbol{p}+\hbar\mathbf{k})^2/2m - \boldsymbol{p}^2/2m$, where $\hbar\omega$ and $\hbar\mathbf{k}$ are the transferred energy and momentum. It follows that the dynamic structure factor takes the form[1,3]

$$S(\mathbf{k},\omega) \propto \left\langle \delta\left(\hbar\omega - \epsilon_k - \boldsymbol{p}\cdot\mathbf{k}/m\right)\right\rangle \propto \mathcal{P}\left[\frac{m}{k}(\hbar\omega-\epsilon_k)\right] , \tag{1.1}$$

where $\epsilon_k = \hbar^2k^2/2m$ and the angular brackets denote the thermal average over the *initial* single-particle momentum distribution in the sample. Then, the measured line shape consists of a peak, centered at the recoil energy ϵ_k, whose form and width do reflect the equilibrium statistical distribution $\mathcal{P}(p_\parallel)$ of $p_\parallel = \boldsymbol{p}\cdot\mathbf{k}/k$, i.e., the component of $\boldsymbol{p}$ in the direction of the momentum transfer. Classically, $\mathcal{P}(p_\parallel)$ is a Gaussian with $\langle p_\parallel^2\rangle = m/\beta$. This makes DINS a very useful tool for the direct measurement of the single-particle kinetic energy, a quantity that is not accessible by other means. Actually, the impulse approximation completely neglects final-state effects, which can to some extent modify the line shape at intermediate momentum transfers.[3–5]

Since from the first significant experiments, the attention of DINS experimentalists has been mostly devoted to the study of strongly quantum systems, like solid helium,[6,7] parahydrogen,[8,9] and, more recently, liquid helium,[10] for which also the role of final-state effects has been experimentally investigated.[11,12] The main motivation was in the interest of looking for the deviation of the momentum distribution and of the kinetic energy from their trivial classical behavior. Therefore, the theoretical interpretation of the data requires quantum calculations. For instance, by path integral Monte Carlo (PIMC) simulations Zoppi and Neumann[13] have given a theoretical counterpart of the DINS data for solid parahydrogen,[9] and the agreement with experiment is surprisingly good in spite of the simple Lennard-Jones (LJ) model interaction between hydrogen molecules.

Recently, Peek, Fujita, Schmidt, and Simmons[14] performed DINS measurements of the momentum distribution of solid neon. In this case the few available theoretical predictions for the kinetic energy at low temperature (Table VI; see also the comparison table in Ref. 14 and the references quoted therein) are lower than the measured values. The above-mentioned authors conclude that the disagreement is due to the fact that the theories are of a harmonic type and that it signalizes the importance of nonlinearity in solid neon.

Thus, one motivation of this paper was to produce theoretical data for rare-gas solids, using Monte Carlo

techniques, in such a way that nonlinearity would be accounted for, overcoming the problems of harmoniclike approaches. In a recent paper[15] we have applied to a model for solid argon a theoretical method, that was previously developed and successfully applied to low-dimensional systems.[16–20] The method is based on the definition of an *effective potential* that is to be dealt with as in classical thermodynamics. Using a Monte Carlo sampling for the effective classical problem we were able to get quantum results with an enormous reduction in the computer time, compared with ordinary PIMC. In Ref. 15 our main goal was to benchmark the usefulness of the effective potential approach by an accurate comparison of PIMC and of effective-potential Monte Carlo (EPMC) data. Similar EPMC computations were also employed by another group[21–23] for models corresponding to rare-gas solids, confirming the power of this method for solid systems with not too strong quantum coupling. This last limitation arises from a kind of *low-coupling* expansion that is needed for eliminating involuted self-consistencies in the evaluation of the effective potential. As a consequence, it turns out that for the strong-coupling case of neon it is more convenient to rely on PIMC results, rather than on EPMC, even though the latter could be improved by taking a higher order in the low-coupling expansion.[23] On the other hand, for heavier rare-gas solids (argon, krypton, xenon) EPMC gives quite accurate results.

In Sec. II we give some details of the PIMC algorithm we used, together with a simple device for improving the extrapolations to the quantum limit of infinite Trotter numbers, and we derive the expression of the average kinetic energy within the effective potential method.

In Sec. III we introduce the model potential and report the details of the PIMC- and of the EPMC simulations we made; the explicit expressions of the effective potential and of the average kinetic energy for the actual three-dimensional solid model are given as well. The results are reported and described in Sec. IV: in particular, the calculated kinetic energy for neon turns out to be lower than the experimental one, and not compatible with the error bars. The main conclusions drawn in Sec. V are that the LJ model seems to be an oversimplification for the behavior of solid neon, and that the kinetic energies of the heavier rare-gas solids are comparable to that of neon, due to the different energy scales of the respective interactions, so that it should be possible to detect them by DINS experiments similar to the one reported in Ref. 14.

II. NUMERICAL AND MATHEMATICAL TECHNIQUES

Before coming to the particular solid-state model which is the subject of this paper, we give in this section some information and remarks about the general techniques we used in the computations.

We refer to a general model system with M degrees of freedom, composed of interacting particles of mass m, with coordinates $(\hat{q}_1,...,\hat{q}_M)\equiv\hat{\boldsymbol{q}}$, and momenta $(\hat{p}_1,...,\hat{p}_M)\equiv\hat{\boldsymbol{p}}$, such that $[\hat{q}_i,\hat{p}_j]=i\hbar\delta_{ij}$. Such a system is ruled by the quantum Hamiltonian operator

$$\hat{\mathcal{H}}(\hat{\boldsymbol{p}},\hat{\boldsymbol{q}}) \equiv K(\hat{\boldsymbol{p}}) + V(\hat{\boldsymbol{q}}) = \sum_{i=1}^{M} \frac{\hat{p}_i^2}{2m} + V(\hat{\boldsymbol{q}}) \ , \qquad (2.1)$$

where $K(\hat{\boldsymbol{p}})=\hat{K}$ is the total kinetic energy and $V(\hat{\boldsymbol{q}})=\hat{V}$ is the interaction potential. The equilibrium density operator of the system at the temperature $T=\beta^{-1}$, is defined as $\hat{\rho}(\beta)=e^{-\beta\hat{\mathcal{H}}}$, and has the matrix elements $\rho(\boldsymbol{q}',\boldsymbol{q};\beta)\equiv\langle\boldsymbol{q}'|e^{-\beta\hat{\mathcal{H}}}|\boldsymbol{q}\rangle$.

A. Path integral Monte Carlo

The PIMC simulations presented in this paper were performed with the usual "primitive algorithm."[24,25] It is based on the semigroup property of the density matrix

$$\rho(\boldsymbol{q}',\boldsymbol{q};\beta) = \prod_{\ell=1}^{P-1}\left(\int d\boldsymbol{q}_\ell\right)\rho(\boldsymbol{q}',\boldsymbol{q}_{P-1};\tau)\rho(\boldsymbol{q}_{P-1},\boldsymbol{q}_{P-2};\tau)\cdots\rho(\boldsymbol{q}_1,\boldsymbol{q};\tau) \ , \qquad (2.2)$$

where $\tau=\beta/P$, and on the approximation at the high temperature τ^{-1} of the density matrix

$$\rho(\boldsymbol{q}',\boldsymbol{q};\tau) = \left(\frac{m}{2\pi\hbar^2\tau}\right)^{M/2}\exp\left(-\frac{m}{2\hbar^2\tau}(\boldsymbol{q}'-\boldsymbol{q})^2 - \frac{\tau}{2}[V(\boldsymbol{q}')+V(\boldsymbol{q})]\right) + O(\tau^2) \ . \qquad (2.3)$$

The integer P is the *Trotter number*, and for $P\to\infty$ the exact quantum results are recovered. Of course, only finite values of it can be considered in PIMC, the computer time needed being proportionally increasing with P. Indeed, by means of the above formulas, the computation of quantum thermal averages is reduced to a classical-like thermal average, but over a system with $M\times P$ degrees of freedom, corresponding to P copies of the original system, interacting with a "quantum" quadratic potential. As for the kinetic energy, it is calculated by PIMC as the average of the "crude" energy estimator:[26–28]

$$\frac{M}{2\tau} - \frac{1}{P}\frac{m}{2\hbar^2\tau^2}\sum_{\ell=1}^{P}(\boldsymbol{q}_\ell-\boldsymbol{q}_{\ell-1})^2 \ . \qquad (2.4)$$

We remark that Eq. (2.3) is based on the free-particle density matrix, so that it can happen that quite large Trotter numbers are required just for describing the quantum harmonic behavior of the system, while the nonharmonic part of the interactions is adequately sampled in PIMC simulations with a comparatively low P. This is indeed true for solid-state systems with low and moderate

quantum coupling, in the low-temperature region, since the quantum anharmonic effects are small compared with the contribution from the harmonic excitations. Noting that the thermodynamic properties of the harmonic oscillator can be calculated analytically also for the finite Trotter number P,[27,29] we are led to improve the PIMC simulation results with the addition of the finite-P corrections for the harmonic approximation of the model system. We then replace the value A_P of any thermodynamic property A, obtained in a PIMC simulation with Trotter number P, with

$$A_P + (A_\infty^{(\mathrm{H})} - A_P^{(\mathrm{H})}) \ , \tag{2.5}$$

where $A_P^{(\mathrm{H})}$ is the exact finite-P result for the harmonic approximation of the model. The above picture has been confirmed to be realistic in the case of solid argon,[15] where this simple device has proven to be very efficient in improving the accuracy of extrapolated quantities to $P\to\infty$: indeed the belief that rising P leads to more and more precise values becomes illusory beyond a certain point, since for higher P the numerical uncertainty increases.

In the present case we have used the finite-P expression for the harmonic kinetic energy at $T=\beta^{-1}$:

$$\left\langle \hat{K} \right\rangle_P^{(\mathrm{H})} = \frac{T}{2} \sum_k \sum_{\ell=1}^{P} \frac{{f_k}^2}{{f_k}^2 + P^2 \sin^2(\pi\ell/P)} \underset{P\to\infty}{\longrightarrow} \frac{T}{2} \sum_k f_k \coth f_k \ , \tag{2.6}$$

where $f_k = \frac{1}{2}\beta\hbar\omega_k$ and ω_k are the frequencies of the harmonic approximation to the model, defined by the secular equation

$$m\,\omega_k^2\ \delta_{kl} = \sum_{ij} U_{ki}\ \partial_i\partial_j V(\boldsymbol{q}_0)\ U_{lj} \ . \tag{2.7}$$

The orthogonal matrix U_{ki} is a Fourier transformation (possibly multiplied by a polarization diagonalization), if the reference configuration $\boldsymbol{q}_0$ is translation invariant.

B. Effective potential method

The Giachetti-Tognetti variational method[16–18,30,31] allows us to define a "global" effective potential $V_{\mathrm{G}}(\boldsymbol{q})$, such that the quantum partition function is at best approximated by the classical-like formula

$$\mathcal{Z} = \left(\frac{m}{2\pi\hbar^2\beta}\right)^{M/2} \int d\boldsymbol{q}\ e^{-\beta V_{\mathrm{G}}(\boldsymbol{q})} \ . \tag{2.8}$$

Without going into the details of the effective potential framework, which has been extensively discussed and applied in other papers (see, e.g., the references quoted above), we note that it shares with the "trick" for the extrapolation of PIMC data described in the previous subsection the underlying general idea of giving exact account for the quantum harmonic part.

For the purposes of this paper we resort to what we have called the *low-coupling approximation* (LCA),[16,17,31–33] in its *first-order* form.[20,15] For a translation invariant system (see, e.g., Refs. 33 and 34) the LCA effective potential reads

$$V_{\mathrm{G}}(\boldsymbol{q}) = V(\boldsymbol{q}) + \frac{1}{\beta}\sum_k \ln\frac{\sinh f_k}{f_k} + \frac{1}{2}\sum_{ij}\alpha_{ij}\left[\partial_i\partial_j V(\boldsymbol{q}) - \partial_i\partial_j V(\boldsymbol{q}_0)\right] \ , \tag{2.9}$$

with $\alpha_{ij} = \sum_k U_{ki}U_{kj}\alpha_k$, where

$$\alpha_k = \frac{\hbar}{2m\omega_k}\left(\coth f_k - \frac{1}{f_k}\right) \tag{2.10}$$

is the pure-quantum (i.e., the difference between quantum and classical) square fluctuation of a harmonic oscillator with frequency ω_k.

In order to yield the expression for the average kinetic energy, one has simply to take the explicit expression for the average of squared momenta,[35] and to perform the LCA exactly as shown in Sec. 3.3 of Ref. 33. Defining the classical-like configuration average with the effective potential,

$$\left\langle f(\boldsymbol{q}) \right\rangle_{\mathrm{G}} \equiv \frac{1}{\mathcal{Z}}\left(\frac{m}{2\pi\hbar^2\beta}\right)^{M/2} \int d\boldsymbol{q}\ e^{-\beta V_{\mathrm{G}}(\boldsymbol{q})}\ f(\boldsymbol{q}) \ , \tag{2.11}$$

the final result is

$$\left\langle \hat{K} \right\rangle = \frac{1}{2m}\sum_k \gamma_k + \sum_{ij}\vartheta_{ij}\left[\left\langle \partial_i\partial_j V(\boldsymbol{q}) \right\rangle_{\mathrm{G}} - \partial_i\partial_j V(\boldsymbol{q}_0)\right], \tag{2.12}$$

with

$$\gamma_k = \tfrac{1}{2} m\hbar\omega_k \coth f_k \tag{2.13}$$

and $\vartheta_{ij} = \sum_k U_{ki}U_{kj}\vartheta_k$, where

$$\vartheta_k = \frac{\hbar}{8m\omega_k}\left(\coth f_k - \frac{f_k}{\sinh^2 f_k}\right) \ . \tag{2.14}$$

The first term in Eq. (2.12) represents the quantum harmonic result, so that the second one arises from quantum nonlinear effects. Indeed, in the classical limit, i.e., for $f_k\to 0$, the correct equipartition result is found, since $\gamma_k\to m/\beta$ and $\vartheta_k\to 0$.

III. MODEL POTENTIAL AND MONTE CARLO SIMULATIONS

As a model for rare-gas solids we consider a system composed of N atoms (pointlike particles in three dimensions without internal degrees of freedom, so that $M=3N$) of mass m, arranged on a three-dimensional fcc lattice with fixed volume (or number density). These atoms are labeled by their classical equilibrium positions $\mathbf{l}\equiv\{l_1,l_2,l_3\}$, and $\boldsymbol{x}_{\mathbf{l}}\equiv\{x_{\mathbf{l}\alpha}\}$ ($\alpha=1,2,3$) is the instantaneous position of the $\mathbf{l}$th atom. The potential energy consists in a pairwise central interaction $u(r)$, so that

the Hamiltonian of the model system is

$$\mathcal{H} = \sum_{\mathbf{l}} \frac{m}{2}\dot{\boldsymbol{x}}_{\mathbf{l}}^2 + \frac{1}{2}\sum_{\mathbf{l},\mathbf{l}'} u(x_{\mathbf{l}\mathbf{l}'}) \ , \tag{3.1}$$

where $\boldsymbol{x}_{\mathbf{l}\mathbf{l}'}=\boldsymbol{x}_{\mathbf{l}}-\boldsymbol{x}_{\mathbf{l}'}$. For the particular form of the pair interaction we choose the widely used Lennard-Jones (LJ) "6-12" potential

$$u(r) = 4\varepsilon\left[\left(\frac{\sigma}{r}\right)^{12} - \left(\frac{\sigma}{r}\right)^{6}\right] \ . \tag{3.2}$$

The parameters ε and σ are adjustable parameters, to be optimized for the description of each rare-gas solid. The values we have used are listed in Table I. They have been taken from the literature, where they have been obtained in such a way to match theoretical predictions and experiments for the sublimation energy and for the density at zero temperature and pressure.[36,37] Clearly, the LJ interaction potential is to be considered merely as an *effective* potential for the description of the real systems, whose "true" interaction is much more complicated (in this respect more realistic potentials have been proposed in Refs. 38–40) and involves many-body irreducible terms. On the other hand, the leading quantum effects are well described by such an effective model. For instance, the experimental equation of state and specific heat of solid argon have been shown to be well reproduced.[15]

The strength of the quantum behavior of the interaction is ruled by a coupling parameter $\lambda=\hbar\Omega/\varepsilon$, which is defined as the ratio between the characteristic quantum energy $\hbar\Omega=\hbar\sqrt{u''(r_{\mathrm{m}})/m}$ of the harmonically approximated pair potential (around its minimum r_{m}), and the overall energy scale ε.[41] For the potential (3.2) $r_{\mathrm{m}}=(2)^{1/6}\sigma$ and $\lambda\simeq 7.56\,\hbar/(\sigma\sqrt{m\varepsilon})$.

In all our Monte Carlo computations we have disregarded the dynamic effect of the interactions beyond the nearest-neighbor (NN) distance, i.e., we have replaced $x_{\mathbf{l}\mathbf{l}'}$ with the equilibrium value $|\mathbf{l}-\mathbf{l}'|$ in the Hamiltonian (3.1), unless $\mathbf{l}$ and $\mathbf{l}'$ are first neighbors. This static approximation is common practice in condensed matter simulations, and allows us to keep the well-established parameters ε and σ, determined for the more realistic case of all-neighbors interaction. In other words, we are dealing with a NN Hamiltonian, plus a volume depending correction, which describes the static potential energy of the long-range interactions. The most important effects that are included in this way are temperature independent additive terms to the average potential energy and to the pressure. In addition, sample calculations allowing for dynamic interactions up to the second neighbor shell were performed but showed no significant differences in the numerical results.

TABLE I. Characteristic parameters of the LJ potential for the rare-gas solids considered in this paper. Values of ε and σ taken from Ref. 37 (Ne), Ref. 36 (Kr, Xe). The values for argon are those already used in Ref. 15, and differ slightly from those of Ref. 36 (namely, ε=119.0 K and σ=3.395 Å). Also reported are the corresponding coupling constants λ and the relevant "natural units" for density, $\rho^* \equiv m/\sigma^3$, and for pressure, $p^* \equiv \varepsilon/\sigma^3$.

	Ne	Ar	Kr	Xe
m (amu)	20.18	39.95	83.80	131.3
ε (K)	36.68	119.8	164.4	231.1
σ (Å)	2.787	3.405	3.638	3.961
λ	0.694	0.223	0.123	0.0768
p^* (bar)	233.9	418.9	471.4	513.4
ρ^* (g cm^{-3})	1.5479	1.6803	2.8900	3.5081

The formalism of the preceding section straightforwardly applies to the model Hamiltonian (3.1). Of course, the simplified notations used in Sec. II must be replaced by those ones suitable for the crystal lattice. For instance, the coordinates q_i (i=1, ..., M) are replaced by $x_{\mathbf{l}\alpha}$ ($\mathbf{l}$ runs over the N lattice sites; α=1, 2, 3 labels the Cartesian components of $\boldsymbol{x}_{\mathbf{l}}$), and the indices k of Sec. II are replaced by $\mathbf{k}\mu$ ($\mathbf{k}\in$ first Brillouin zone; μ=1, 2, 3 is the polarization index).

Then, for our fcc lattice model (3.1) with dynamic interaction limited to the nearest neighbors, and with a fixed particle density corresponding to an average NN distance d, the frequencies of the harmonic excitations are defined as the solutions of the secular equation

$$\omega_{\mathbf{k}\mu}^2\,\delta_{\mu\nu} = \sum_{\alpha,\beta} \epsilon_{\mu\alpha}(\mathbf{k})\;\omega_{\mathbf{k},\alpha\beta}^2\;\epsilon_{\nu\beta}(\mathbf{k}) \ , \tag{3.3}$$

where $\boldsymbol{\epsilon}_{\mu}(\mathbf{k})=\{\epsilon_{\mu\alpha}(\mathbf{k})\}$ are the polarization vectors and

$$\omega_{\mathbf{k},\alpha\beta}^2 = \frac{1}{m}\frac{\partial^2}{\partial_{x_\alpha}\partial_{x_\beta}} u\Big(|\boldsymbol{x}|=d\Big) \sum_{\mathbf{d}} 2\sin^2\frac{\mathbf{k}\cdot\mathbf{d}}{2} \ , \tag{3.4}$$

with $\mathbf{d}$ running over the 12 first neighbors, is the dynamic matrix (see also Ref. 15).

In this paper we report results only for the zero-pressure state. At each temperature, the thermodynamic state of zero pressure has been reached — with an accuracy of less than 6 bars (35 bars for neon), which is practically zero in solid-state systems — by slightly varying the lattice constant in successive test runs, taking into account the experimental compressibilities. The maximum deviation from the experimental densities is found to be very small, thanks to the above-mentioned cut-off correction to the pressure.

Monte Carlo simulations with the effective potential (EPMC), i.e., for the distribution (2.11) (see also Refs. 15, 22 and 23), were made for the rare-gas solids with lower coupling ($\lambda\ll 1$). The usefulness of this approach has been carefully verified in Ref. 15, where the EPMC technique has been extensively tested against path integral Monte Carlo (PIMC) computations for the case of argon ($\lambda\simeq 0.22$). In the stronger coupling case of neon ($\lambda\simeq 0.7$) the EPMC is less convenient since the full "second-order" approach has to be used,[23] and we preferred to rely on PIMC simulations, with the improved extrapolation procedure (2.5).

In both EPMC and PIMC the sample consisted of an fcc lattice of 108 atoms enclosed in a cubical box, with periodic boundary conditions, and the simulations were based on the Metropolis algorithm and single-particle moves.[26] The maximum displacement was chosen such

as to lead to an acceptance ratio of 30–50 % of the trial moves. Each run was started from a perfect fcc lattice at the appropriate density and equilibrated for a suitable number of steps (trial moves per particle), depending on the specific Monte Carlo technique used.

In the PIMC simulations we varied the Trotter number P between 4 and 32, and and each run consisted of 50 000 steps for equilibration and 450 000 steps of further run, during which the averages were accumulated every tenth configuration.

The EPMC simulations consisted of 25 000 steps each (after 2500 equilibration steps), with every fifth configuration taken for calculating averages. Due to its temperature and density dependence, the effective potential has to be recalculated for each thermodynamic state. However, the time required for this is entirely negligible compared to the total simulation time. The actual expression for the effective potential is easily found from Eq. (2.9):

$$V_{\rm G}\left(\{\boldsymbol{x}_{\rm l}\}\right)=\frac{1}{2}\sum_{|{\rm l}-{\rm l}'|=d}u_{\rm G}(x_{{\rm l}{\rm l}'})+\frac{1}{2}\sum_{|{\rm l}-{\rm l}'|>d}u\left(|{\rm l}-{\rm l}'|\right)+\frac{1}{\beta}\sum_{\mathbf{k},\mu}\ln\frac{\sinh f_{\mathbf{k}\mu}}{f_{\mathbf{k}\mu}}\ . \tag{3.5}$$

The aforementioned static approximation for the interaction beyond the first neighbors is explicitly shown, while the NN effective pair interaction is

$$u_{\rm G}(r)=u(r)+\tfrac{1}{2}\left[u''(r)-u''(d)\right]\alpha_{\rm L}+\frac{1}{2}\left(\frac{u'(r)}{r}-\frac{u'(d)}{d}\right)\alpha_{\rm T}, \tag{3.6}$$

and $\alpha_{\rm L}$ and $\alpha_{\rm T}$ are, respectively, the longitudinal and transverse renormalization parameters:

$$\alpha_{\rm L}=\frac{1}{N}\sum_{\mathbf{k},\mu}4\sin^2\frac{\mathbf{k}\cdot\mathbf{d}}{2}\left(\frac{\mathbf{d}\cdot\boldsymbol{\epsilon}_\mu(\mathbf{k})}{d}\right)^2\alpha_{\mathbf{k}\mu}\ , \tag{3.7}$$

$$\alpha_{\rm T}=\frac{1}{N}\sum_{\mathbf{k},\mu}4\sin^2\frac{\mathbf{k}\cdot\mathbf{d}}{2}\left[1-\left(\frac{\mathbf{d}\cdot\boldsymbol{\epsilon}_\mu(\mathbf{k})}{d}\right)^2\right]\alpha_{\mathbf{k}\mu}\ . \tag{3.8}$$

Eventually, Eq. (2.12) is put in explicit form in terms of the parameters $\vartheta_{\rm L,T}$ (defined in the same way as $\alpha_{\rm L,T}$, with $\alpha_{\mathbf{k}\mu}$ replaced by $\vartheta_{\mathbf{k}\mu}$):

$$\left\langle\hat{K}\right\rangle=\frac{1}{2m}\sum_k\gamma_k+\frac{1}{2}\sum_{|{\rm l}-{\rm l}'|=d}\left\{[\langle u''(x_{{\rm l}{\rm l}'})\rangle_{\rm G}-u''(d)]\vartheta_{\rm L}+\left[\left\langle\frac{u'(x_{{\rm l}{\rm l}'})}{x_{{\rm l}{\rm l}'}}\right\rangle_{\rm G}-\frac{u'(d)}{d}\right]\vartheta_{\rm T}\right\}\ . \tag{3.9}$$

The calculation of the quantum average kinetic energy per atom, $e_{\rm K}\equiv\langle\hat{K}\rangle/N$, by means of Monte Carlo evaluation of the classical-like averages with the effective potential appearing on the right-hand side of Eq. (3.9) is what we have indeed called EPMC. Since the effective potential depends on temperature as well as on density it is not possible to use the standard classical expression[26] for the calculation of the pressure p. Rather, one has to rederive the microscopic expression to be averaged, by starting from the thermodynamic relationship $p=\beta^{-1}\partial\ln\mathcal{Z}/\partial V$, and taking explicitly into account the dependence on the equilibrium lattice spacing d, arising through Eqs. (3.3) and (3.4), of the renormalization parameters $\alpha_{\rm L,T}$ and of the logarithmic term in $V_{\rm G}$. The same holds for other quantities, like internal energy, specific heats, compressibilities, which are not considered in this paper.

IV. RESULTS AND DISCUSSION

In Table I the characteristic parameters we used for the four rare-gas solids (neon, argon, krypton, and xenon) are reported. The values of the LJ parameters ε and σ have been taken from Ref. 37 for neon, from Ref. 36 for krypton and xenon, whereas their values for argon are those already used in Ref. 15 (determined in Ref. 42 from the high-temperature gas-phase data, they differ slightly from those of Ref. 36, namely, ε=119.0 K and σ=3.395 Å).

TABLE II. Solid LJ neon at $T=5$, 10, 15, and 20 K: PIMC results for pressure p and kinetic energy per atom $e_{\rm K}$, at the fixed values of the density ρ reported in the first row. All the values are inclusive of the harmonic correction as in Eq. (2.5). The extrapolated values are listed as $P=\infty$. "Natural units" ρ^*, p^*, ε from Table I. The absolute value of the extrapolated pressure is always less than $0.09\,p^*\sim 20$ bars.

	$T=5$ K $\rho_{\rm exp}=0.9735\,\rho^*$ $\rho=0.9650\,\rho^*$		$T=10$ K $\rho_{\rm exp}=0.9710\,\rho^*$ $\rho=0.9630\,\rho^*$		$T=15$ K $\rho_{\rm exp}=0.9628\,\rho^*$ $\rho=0.9550\,\rho^*$		$T=20$ K $\rho_{\rm exp}=0.9477\,\rho^*$ $\rho=0.9440\,\rho^*$	
P	p/p^*	$e_{\rm K}/\varepsilon$	p/p^*	$e_{\rm K}/\varepsilon$	p/p^*	$e_{\rm K}/\varepsilon$	p/p^*	$e_{\rm K}/\varepsilon$
4	-0.397	0.919 ± 0.001	-0.406	1.005 ± 0.005	-0.316	1.107 ± 0.002	-0.104	1.236 ± 0.002
8	-0.435	0.981 ± 0.001	-0.290	1.083 ± 0.002	-0.191	1.168 ± 0.003	-0.059	1.286 ± 0.005
16	-0.313	1.062 ± 0.002	-0.192	1.132 ± 0.005	-0.160	1.199 ± 0.008	-0.002	1.300 ± 0.009
24	-0.239	1.094 ± 0.003	-0.170	1.141 ± 0.007	-0.136	1.202 ± 0.012	0.002	1.302 ± 0.015
32	-0.189	1.111 ± 0.005	-0.118	1.161 ± 0.010	-0.130	1.213 ± 0.015	0.001	1.300 ± 0.020
∞	-0.03	1.167 ± 0.011	-0.04	1.178 ± 0.015	-0.09	1.218 ± 0.020	0.00	1.300 ± 0.025

The results of our calculations are reported in Tables II–V and Figs. 1–3. Most quantities are given in dimensionless form, by reducing them with respect to the "natural units" induced by the mass m, the energy ε, and the length σ. For density and pressure they are $\rho^* \equiv m/\sigma^3$ and $p^* \equiv \varepsilon/\sigma^3$, whose CGS values are also reported in Table I. The equilibrium NN spacing d is related with the reduced density by $\rho/\rho^* = (d/r_m)^{-3}$, r_m being the minimum of the LJ potential (3.2), so that the reduced density ρ/ρ^* at zero pressure reasonably turns out to be close to 1. The zero-pressure density is determined by competing effects, namely, the attractive interaction due to the interactions beyond first neighbors, which tends to increase the density, and the (quantum and thermal) fluctuations, which enhance the repulsive part and thus push to lower density. At the lowest temperatures the only pure-quantum fluctuations do matter, so that the reduced density is expected to be smaller the higher the coupling, as it indeed happens. Remarkably, the maximum deviation of the calculated densities from the experimental ones at all temperatures is always less than 0.3% (0.9% for neon).

In Table II we report the results for the kinetic energy e_K and the pressure p from the PIMC simulations made for neon, at the selected temperatures T = 10, 20, 30, and 40 K, and at the indicated densities. The latter have been chosen through successive trial test runs in order to get a practically vanishing pressure (of course, this procedure is limited by the available computer time). Since the PIMC results have to be extrapolated to infinite Trotter number P, separate runs were done with P=4, 8, 16, 24, and 32. When plotted as a function of $1/P$, the finite-P values usually fall on a smooth curve, which tends to a rather well-defined limit as $1/P \to 0$. The data of Table II are inclusive of the "harmonic correction" introduced at the end of Sec. II A, Eq. (2.5), and the last row, marked "∞," refers to the extrapolated values, obtained by a quadratic fit to the points at $P \geq 8$. The qualitative improvement in the extrapolation of the "harmonic corrected" PIMC data at 5 K is made apparent in Fig. 1, where also the raw PIMC data are reported for comparison. Even for low Trotter numbers the corrected PIMC results are now closer to the quantum mechanical limit, and the extrapolated values are in good agreement with the extrapolation of the bare PIMC results.

In Tables III–V the EPMC data for the kinetic energy per atom e_K of solid argon, krypton, and xenon are reported. Due to the much lower computational weight, the EPMC computations have been made for many temperatures. In addition it has been possible to get closer to the zero-pressure state ($p \simeq 0 \pm 6$ bars) by means of preliminary runs devoted to adjust the corresponding densities. The reported uncertainties are those arising from the numerical MC simulations. A systematic uncertainty is, of course, embodied in the variational calculations that lead to the effective-potential method, which just for this reason has been tested for many "toy models."[16–20]

In Fig. 2 these densities can be compared with the experimental ones (their values, ρ_{exp}, are reported in the second column of Tables III–V). The agreement with the experimental equation of state of these rare-gas solids appears almost perfect, if one considers that we have used the simple LJ model (3.2), with the non-nearest-neighbor interaction treated in the static approximation

TABLE III. Solid LJ argon: EPMC results for the kinetic energy per atom e_K at different temperatures, for the fixed density values reported in the third column, for which the calculated pressures are $p = 0 \pm 0.01\,p^* = 0 \pm 2$ bars (see text). The second column (ρ_{exp}) reports the experimental values from Ref. 46.

T (K)	ρ_{exp}/ρ^*	ρ/ρ^*	e_K/ε
4	1.0540	1.0523	0.3830 ± 0.0007
10	1.0535	1.0522	0.3920 ± 0.0013
15	1.0525	1.0509	0.4106 ± 0.0019
20	1.0500	1.0487	0.4360 ± 0.0026
25	1.0467	1.0449	0.4720 ± 0.0030
30	1.0426	1.0408	0.5130 ± 0.0042
40	1.0326	1.0304	0.6080 ± 0.0049
50	1.0207	1.0181	0.7120 ± 0.0054
60	1.0070	1.0045	0.8230 ± 0.0071
75	0.9825	0.9804	0.9950 ± 0.0092

TABLE IV. Solid LJ krypton: EPMC results for the kinetic energy per atom e_K at different temperatures, for the fixed-density values reported in the third column, for which the calculated pressures are $p = 0 \pm 0.011\,p^* = 0 \pm 5$ bars (see text). The second column (ρ_{exp}) reports the experimental values from Ref. 46.

T (K)	ρ_{exp}/ρ^*	ρ/ρ^*	e_K/ε
4	1.07015	1.06985	0.2207 ± 0.0004
10	1.06961	1.06917	0.2284 ± 0.0009
15	1.06825	1.06764	0.2452 ± 0.0012
20	1.06606	1.06523	0.2704 ± 0.0021
25	1.06323	1.06220	0.3014 ± 0.0021
30	1.05996	1.05857	0.3361 ± 0.0033
40	1.05248	1.05076	0.4126 ± 0.0035
50	1.04417	1.04204	0.4944 ± 0.0041
60	1.03426	1.03230	0.5791 ± 0.0048
75	1.02028	1.01655	0.7092 ± 0.0059

TABLE V. Solid LJ xenon: EPMC results for the kinetic energy per atom e_K at different temperatures, for the fixed-density values reported in the third column, for which the calculated pressures are $p = 0 \pm 0.012\,p^* = 0 \pm 6$ bars (see text). The second column (ρ_{exp}) reports the experimental values from Ref. 46.

T (K)	ρ_{exp}/ρ^*	ρ/ρ^*	e_K/ε
5	1.0782	1.0781	0.1399 ± 0.0003
10	1.0779	1.0776	0.1458 ± 0.0009
15	1.0771	1.0764	0.1598 ± 0.0012
20	1.0758	1.0745	0.1798 ± 0.0011
25	1.0741	1.0721	0.2035 ± 0.0014
30	1.0713	1.0696	0.2297 ± 0.0015
40	1.0665	1.0641	0.2863 ± 0.0021
50	1.0604	1.0579	0.3459 ± 0.0029
60	1.0534	1.0513	0.4072 ± 0.0042
75	1.0419	1.0416	0.5009 ± 0.0046

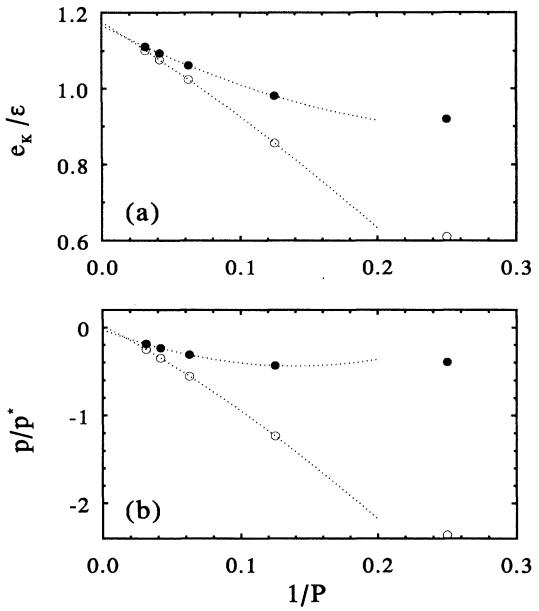

FIG. 1. (a) Kinetic energy per atom e_K and (b) pressure p of solid neon, vs the reciprocal Trotter number $1/P$, at $T = 5$ K and $\rho = 0.9650\rho^* = 1.4937\,\mathrm{g\,cm^{-3}}$. Open circles: raw PIMC data; solid circles: PIMC data plus the harmonic correction as in Eq. (2.5). The dotted lines are quadratic χ^2 fits to the points $P \geq 8$, drawn in order to extrapolate to $P=\infty$.

(see Sec. III). For the purpose of this paper a good reproduction of the equation of state is very important, since the average kinetic energy strongly depends upon density: In the Debye approximation $\Delta\varepsilon_K/\varepsilon_K \simeq \gamma_L \Delta\rho/\rho$, with γ_L a lumped Grüneisen constant, so that the uncertainty in the density corresponds to a possibly higher uncertainty for ε_K.

The temperature behavior of the kinetic energy per atom is plotted in Fig. 3, using the reduced units for both axes. In this way one obtains a representation which depends only upon the coupling constant λ, so that the deviation from the classical behavior $e_K = (3/2)T$ is larger the larger the coupling. In Fig. 3, indeed, the largest deviation occurs in the case of neon, and the heavier rare-gas solids (krypton and xenon) seem to behave more and more classically. Remarkably, using dimensionful units, the same data bear the quite different aspect reported in Fig. 4. This is due to the increasing energy scales ε corresponding to the interaction of heavier rare-gas atoms (see

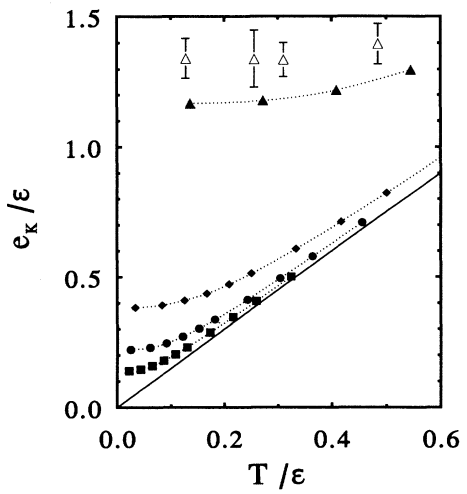

FIG. 3. Reduced kinetic energy per atom e_K/ε of solid LJ neon (solid triangles), argon (diamonds), krypton (circles), and xenon (squares), vs reduced temperature T/ε. This scaling (see Table I) gives a representation depending only on the coupling constant λ (e.g., at $T\to 0$, $e_K/\varepsilon \sim 1.7\lambda$). The solid line is the classical result $e_K = (3/2)T$, the open triangles are experimental data for neon from Ref. 14.

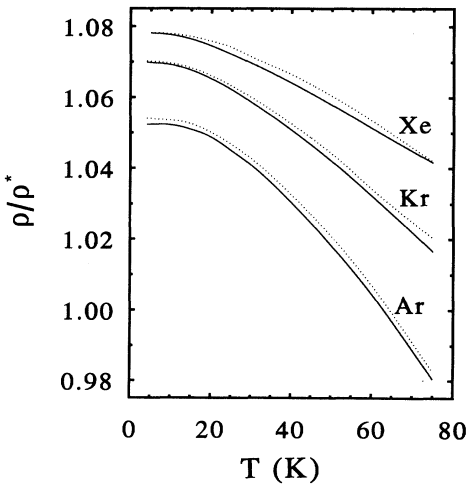

FIG. 2. Calculated reduced densities ρ/ρ^* for argon, krypton, and xenon, vs temperature. The curves do interpolate the calculated (solid lines) and the experimental (dotted lines) point data reported in Tables III–V.

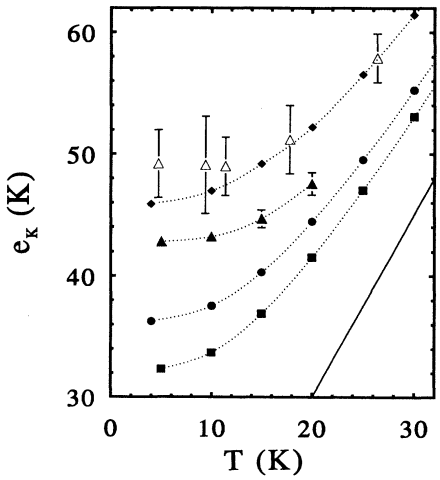

FIG. 4. Kinetic energy per atom e_K vs temperature. Symbols and lines as in Fig. 3. It is apparent that, in dimensionful units, the quantum kinetic energies at low temperatures are comparable, in spite of the quite different quantum couplings.

TABLE VI. Comparison among various results for the kinetic energy of rare-gas solids at $T = 0$. The experimental and calculated nearest-neighbor distances d are also reported. Bernardes uses the values $\sigma = 2.74$, 3.40, 3.65, and 3.98 Å, and $\varepsilon = 36.2$, 121.0, 163.0, and 231.8 (K) for neon, argon, krypton, and xenon, respectively. Nosanow and Shaw (Ref. 44) use the same σ and ε, as well as the same densities obtained by Bernardes. See also the discussion made in Sec. IV.

	Neon		Argon		Krypton		Xenon	
	d (Å)	e_K (K)	d (Å)	e_K (K)	d (Å)	e_K (K)	d (Å)	e_K (K)
Experiment (Ref. 46)	3.156	49[a]	3.755		3.992		4.336	
Bernardes (Ref. 43)	3.13	47.9	3.76	54.7	4.01	40.2	4.35	37.2
Nosanow and Shaw (Ref. 44)		42.8		48.8		36.8		32.7
Present work	3.16	42.8 ± 0.4	3.76	45.5	3.99	36.2	4.34	32.1

[a]Reference 14.

Table I). Paradoxically, solid argon displays a kinetic energy per atom larger than that of neon at the same temperature, and for krypton and xenon e_K appears to be of the same order of magnitude. As a remarkable consequence, such large quantum effects should be measurable for *all* rare-gas solids, including krypton and xenon, by means of the deep-inelastic neutron scattering technique.

The experimental data for solid neon, from Ref. 14, are also reported in Figs. 3 and 4. They appear to be systematically higher than our theoretical results, even if the given error bars are of the order of the deviation from our results.

In Table VI we compare data for the zero-pressure nearest-neighbor spacing d and kinetic energy at $T = 0$. Reported are experimental outcomes and the results of previous calculations by Bernardes[43] (variational with trial wave function) and by Nosanow and Shaw[44] (self-consistent solution of Hartree equations). In both papers a LJ all-neighbors model is used, with interaction parameters as reported in the table caption, and in the second paper the same density values obtained in the first one have been used. For the kinetic energy, our results are generally close to those by Nosanow and Shaw, whereas Bernardes found much higher values. This disagreement can be perhaps attributed to the rough trial wave function he used.

However, in the case of neon, the above-mentioned DINS experiment[14] agrees with Bernardes result. Our opinion is that this agreement is incidental, and that the correct results for the "all-neighbors LJ crystal" are those we have reported. This judgment is confirmed by the results by Nosanow and Shaw (even though a significant deviation is still there for argon), and also by the self-consistent approximation approach by Koehler[45] (yielding ε_K=42.6 K). The disagreement with the real rare-gas solid should be due to the oversimplification of the LJ model, which neglects the fine features of the true interaction potential, as well as many-body interactions.

V. CONCLUSION

In this paper we have reported Monte Carlo results for the quantum kinetic energy per atom of the rare gas solids of neon, argon, krypton, and xenon. We have used the Giachetti-Tognetti *effective potential* method[16] in order to reduce the computational effort: indeed that method yields classical-like expressions for quantum averages, that we have evaluated by standard Monte Carlo simulation (EPMC). The usefulness of EPMC has already been proven in a preceding paper.[15] In the strong-coupling case of neon we have performed path integral Monte Carlo (PIMC) simulations, for which an improved method for the extrapolation to infinite Trotter number, Eq. (2.5), has been implemented.

The interaction potential was chosen of the Lennard-Jones form, and the interaction between non-nearest-neighbors has been taken into account in a static approximation. Then, the simulations have been performed at the zero-pressure state, whose density has been determined by preliminary test runs. The resulting temperature behavior of the density is in quite good agreement with the experimental equation of state for all the four rare-gas solids.

The results for the kinetic energy per atom e_K show that even for argon, krypton, and xenon the quantum effects are quite evident, in spite of their "almost classical" character, due to the different energy scales characterizing their interaction. The deviation of the kinetic energy per atom should be directly detectable by deep-inelastic neutron scattering (DINS). As for the recent DINS results for neon,[14] there is no quantitative agreement with our results, maybe due to the oversimplification of the LJ model.

ACKNOWLEDGMENT

We would like to thank Professor R.O. Simmons for interesting and helpful discussions about the subject of this work.

[1]P.C. Hohenberg and P.M. Platzmann, Phys. Rev. **152**, 198 (1966).
[2]V.F. Sears, Phys. Rev. **185**, 200 (1969).
[3]V.F. Sears, Phys. Rev. B **30**, 44 (1984).
[4]A. Belić and V.R. Pandharipande, Phys. Rev. B **39**, 2696 (1989).
[5]R.N. Silver, Phys. Rev. B **38**, 2283 (1988).
[6]R.O. Hilleke, P. Chaddah, R.O. Simmons, D.L. Price, and S.K. Sinha, Phys. Rev. Lett. **52**, 847 (1984).
[7]P.E. Sokol, D.A. Peek, R.O. Simmons, D.L. Price, and R.O.

Hilleke, Phys. Rev. B **33**, 7787 (1986).
[8]W. Langel, D.L. Price, R.O. Simmons, and P.E. Sokol, Phys. Rev. B **38**, 11 275 (1988).
[9]M.F. Herwig, J.L. Gavilano, M.C. Schmidt, and R.O. Simmons, Phys. Rev. B **41**, 96 (1990).
[10]M.F. Herwig, P.E. Sokol, T.R. Sosnick, W.M. Snow, and R.C. Blasdell, Phys. Rev. B **41**, 103 (1990).
[11]M.F. Herwig, P.E. Sokol, W.M. Snow, and R.C. Blasdell, Phys. Rev. B **44**, 308 (1991).
[12]T.R. Sosnick, W.M. Snow, R.N. Silver, and P.E. Sokol, Phys. Rev. B **43**, 216 (1991).
[13]M. Zoppi and M. Neumann, Phys. Rev. B **43**, 10 242 (1991).
[14]D.A. Peek, I. Fujita, M.C. Schmidt, and R.O. Simmons, Phys. Rev. B **45**, 9680 (1992).
[15]A. Cuccoli, A. Macchi, M. Neumann, V. Tognetti, and R. Vaia, Phys. Rev. B **45**, 2088 (1992).
[16]R. Giachetti and V. Tognetti, Phys. Rev. Lett. **55**, 912 (1985).
[17]R. Giachetti and V. Tognetti, Phys. Rev. B **33**, 7647 (1986).
[18]R.P. Feynman and H. Kleinert, Phys. Rev. A **34**, 5080 (1986).
[19]R. Vaia and V. Tognetti, Int. J. Mod. Phys. B **4**, 2005 (1990).
[20]A. Cuccoli, V. Tognetti, and R. Vaia, Phys. Rev. B **41**, 9588 (1990).
[21]S. Liu, G.K. Horton, and E.R. Cowley, Phys. Lett. A **152**, 79 (1991).
[22]S. Liu, G.K. Horton, and E.R. Cowley, Phys. Rev. B **44**, 11 714 (1991).
[23]S. Liu, G.K. Horton, E.R. Cowley, A.R. McGurn, A.A. Maradudin, and R.F. Wallis, Phys. Rev. B **45**, 9716 (1992).
[24]M. Takahashi and M. Imada, J. Phys. Soc. Jpn. **53**, 963 (1984).
[25]D. Chandler and P.G. Wolynes, J. Chem. Phys. **74**, 4078 (1981).
[26]M.P. Allen and D.J. Tildesley, *Computer Simulation of Liquids* (Clarendon, Oxford, 1987).
[27]M.F. Herman, E.J. Bruskin, and B.J. Berne, J. Chem. Phys. **76**, 5150 (1982).
[28]K. Singer and W. Smith, Mol. Phys. **64**, 1215 (1988).
[29]K.S. Schweizer, R.M. Stratt, D. Chandler, and P.G. Wolynes, J. Chem. Phys. **75**, 1347 (1981).
[30]W. Janke, in *Path Integrals from meV to MeV*, edited by V. Sa-Yakanit *et al.* (World Scientific, Singapore, 1989), pp. 355–365
[31]R. Giachetti, V. Tognetti, A. Cuccoli, and R. Vaia, in *Ordering Phenomena in Condensed Matter*, edited by Z. Galasiewicz (World Scientific, Singapore, 1990), pp. 445–466.
[32]A. Cuccoli, V. Tognetti, P. Verrucchi, and R. Vaia, Phys. Rev. A **45**, 8418 (1992).
[33]A. Cuccoli, A.A. Maradudin, A.R. Mc Gurn, V. Tognetti, and R. Vaia, Phys. Rev. B **46**, 8839 (1992).
[34]A. Cuccoli, V. Tognetti, and R. Vaia, Phys. Rev. A **44**, 2734 (1991).
[35]A particular case of Eq. (36) of Ref. 33.
[36]G.K. Horton, in *Rare Gas Solids*, edited by M.L. Klein and J.A. Venables (Academic, London, 1976), p. 1.
[37]J.S. Brown, Proc. Phys. Soc. **89**, 987 (1966).
[38]J.A. Barker, in *Rare Gas Solids* (Ref. 36), p. 212.
[39]R.A. Aziz and H.H. Chen, J. Chem. Phys. **67**, 5719 (1977).
[40]R.A. Aziz, in *Inert gases*, edited by M.L. Klein (Springer Verlag, Berlin, 1984), p. 5.
[41]The parameter λ defined here better represents the "degree of quanticity" than the so-called de Boer's parameter, $\Lambda=\hbar/(\sigma\sqrt{m\varepsilon})$, used by other authors, since the low-coupling condition is $\lambda \lesssim 1$.
[42]A. Michels, Hub. Wijiker, and H.H. Wijker, Physica **15**, 627 (1949).
[43]N. Bernardes, Phys. Rev. **112**, 1534 (1958).
[44]L.H. Nosanow and G.L. Shaw, Phys. Rev. **128**, 546 (1962).
[45]T.R. Koehler, Phys. Rev. Lett. **17**, 89 (1966).
[46]P. Korpiun and E. Lüscher, in *Rare Gas Solids* (Ref. 36), p. 729.